Pd@Pt Core−Shell Concave Decahedra: A Class of Catalysts for the Oxygen Reduction Reaction with Enhanced Activity and Durability

Xue Wang,[†,‡] Madeline Vara,[§] Ming Luo,[†] Hongwen Huang,[†] Aleksey Ruditskiy,[§] Jinho Park,[§] Shixiong Bao,[†,‡] Jingyue Liu,[∥] Jane Howe,[⊥] Miaofang Chi,[#] Zhaoxiong Xie,[‡] and Younan Xia*[,†,§]

[†]The Wallace H. Coulter Department of Biomedical Engineering, Georgia Institute of Technology and Emory University, Atlanta, Georgia 30332, United States

[‡]State Key Laboratory of Physical Chemistry of Solid Surfaces, Collaborative Innovation Center of Chemistry for Energy Materials, and Department of Chemistry, Xiamen University, Xiamen, Fujian 361005, People's Republic of China

[§]School of Chemistry and Biochemistry, Georgia Institute of Technology, Atlanta, Georgia 30332, United States

[∥]Department of Physics, Arizona State University, Tempe, Arizona 85287, United States

[⊥]Hitachi High-Technologies Canada, Toronto, Ontario M9W 6A4, Canada

[#]Center for Nanophase Materials Sciences, Oak Ridge National Laboratory, Oak Ridge, Tennessee 37831, United States

S *Supporting Information*

ABSTRACT: We report a facile synthesis of multiply twinned Pd@Pt core−shell concave decahedra by controlling the deposition of Pt on preformed Pd decahedral seeds. The Pt atoms are initially deposited on the vertices of a decahedral seed, followed by surface diffusion to other regions along the edges/ridges and then across the faces. Different from the coating of a Pd icosahedral seed, the Pt atoms prefer to stay at the vertices and edges/ridges of a decahedral seed even when the deposition is conducted at 200 °C, naturally generating a core−shell structure covered by concave facets. The nonuniformity in the Pt coating can be attributed to the presence of twin boundaries at the vertices, as well as the

{100} facets and twin defects along the edges/ridges of a decahedron, effectively trapping the Pt adatoms at these high-energy sites. As compared to a commercial Pt/C catalyst, the Pd@Pt concave decahedra show substantial enhancement in both catalytic activity and durability toward the oxygen reduction reaction (ORR). For the concave decahedra with 29.6% Pt by weight, their specific ($1.66 \ mA/cm^2_{Pt}$) and mass ($1.60 \ A/mg_{Pt}$) ORR activities are enhanced by 4.4 and 6.6 times relative to those of the Pt/C catalyst ($0.36 \ mA/cm^2_{Pt}$ and $0.32 \ A/mg_{Pt}$, respectively). After 10 000 cycles of accelerated durability test, the concave decahedra still exhibit a mass activity of $0.69 \ A/mg_{Pt}$, more than twice that of the pristine Pt/C catalyst.
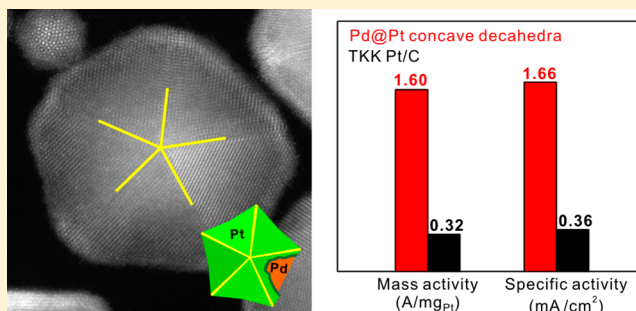
INTRODUCTION

Although proton exchange membrane fuel cells (PEMFCs) offer a promising route to clean energy, it remains challenging to commercialize this technology on an industrial scale due to the high costs associated with such devices. The prohibitive cost of a PEMFC can be largely attributed to the Pt catalyst that is deposited on the cathode to accelerate the sluggish kinetics of the oxygen reduction reaction (ORR).[1] Platinum is the most effective catalyst for ORR,[2] but its abundance in Earth's crust is extremely low. The price of Pt typically doubles every decade due to the ever-growing demand of this precious metal in the automotive industry for the manufacturing of catalytic converters. The catalysts currently used for PEMFCs are based on 3−5 nm Pt nanoparticles, which are poorly defined in terms of facet or surface structure.[3] Because of the low specific activity and poor stability inherent to such tiny particles, a large amount (typically, 0.1−0.2 g per cm^2) of Pt has to be deposited on the cathode of a PEMFC, accounting for 80% of the device

cost. According to a 2014 report from the Department of Energy, the electrocatalyst used in a commercial PEMFC should have a mass activity of at least $0.44 \ A/mg_{Pt}$ by 2020.[4] To achieve this goal, many different types of Pt-based nanocrystals have been developed with improved activity toward ORR by engineering their size, shape, structure, and composition.[5−12]

Deposition of Pt as ultrathin shells onto nanocrystals made of a less expensive and/or more abundant metal has been actively explored as one of the approches.[13−20] To this end, both electrochemical and chemical procedures have been developed for generating the core−shell structures. Monolayers and submonolayers of Pt atoms, for example, have been deposited on nanocrystals made of Pd or other transition metals through a galvanic replacement reaction with the under-potentially deposited Cu shells. Catalysts prepared using this

approach have demonstrated greatly enhanced mass activity toward ORR.[13−17] Most recently, our group has synthesized Pd@Pt core−shell nanocrystals with different surface structures by chemically depositing Pt as conformal shells on Pd nanocrystals with a cubic, octahedral, or icosahedral shape.[18−20] The thickness of the Pt shells can be readily tuned from one to six atomic layers, and the resultant catalysts showed marked enhancement in activity and durability relative to a commercial Pt/C catalyst. Interestingly, when we sought to extend the Pt coating procedure to Pd decahedral seeds with a multiply twinned structure similar to that of an icosahedron, we observed a completely different phenomenon. Instead of forming a conformal, uniform shell, as in the case of an icosahedral seed, the Pt atoms preferentially stay at the vertices and edges of a decahedral seed to create an ultrathin Pt shell covered by concave facets.

It is well established that the surface structure of a nanocrystal plays one of the most important roles in determining its catalytic activity and/or selectivity.[21] In recent years, metal nanocrystals with concave surfaces have attracted increasing attention due to the presence of high-index facets and thus high densities of steps, edges, kinks, and low-coordinated surface atoms.[22−24] Here, we demonstrate that high-index facets could be integrated with twin defects in a novel type of core−shell structure for the fabrication of cost-effective catalysts with substantial enhancement in both specific and mass activities toward ORR. We have also systematically investigated the experimental conditions and thus the mechanistic details responsible for the formation of Pd@Pt core−shell decahedra with concave facets on the surface.

EXPERIMENTAL SECTION

Chemicals and Materials. Ethylene glycol (EG, lot no. L05B13) was purchased from J. T. Baker. Sodium palladium(II) tetrachloride (Na$_2$PdCl$_4$, 99.998%), sodium platinum(IV) hexachloride hexahydrate (Na$_2$PtCl$_6$·6H$_2$O, 98%), poly(vinylpyrrolidone) (PVP, MW ≈ 55 000), L-ascorbic acid (AA), potassium bromide (KBr), ferric chloride (FeCl$_3$), sodium sulfate (Na$_2$SO$_4$), diethylene glycol (DEG, lot no. BCBL9535 V), hydrochloric acid (HCl, 37%), acetic acid (99.7%), and perchloric acid (HClO$_4$, 70%, PPT grade, Veritas) were all obtained from Sigma-Aldrich. All chemicals were used as received. All aqueous solutions were prepared using deionized (DI) water with a resistivity of 18.2 MΩ cm.

Synthesis of Pd Decahedra. The Pd decahedra of 19 nm in size were synthesized using a recently reported protocol.[25] Specifically, 80 mg of PVP and 44 mg of Na$_2$SO$_4$ were dissolved in 2.0 mL of DEG hosted in a 20 mL vial and heated at 105 °C for 10 min in an oil bath under magnetic stirring. Subsequently, 15.5 mg of Na$_2$PdCl$_4$ was dissolved in 1.0 mL of DEG and added into the vial using a pipet. The vial was then capped and maintained at 105 °C for 3 h. The product was collected through centrifugation, washed once with acetone and twice with DI water to remove excess PVP and ionic species, and redispersed in 3 mL of EG.

Synthesis of Pd@Pt Core−Shell Concave Decahedra. For the concave decahedra with a weight percentage (wt %) of 29.6% Pt, 1.0 mL of the suspension of Pd decahedral seeds (0.54 mg/mL), 54 mg of KBr, 66 mg of PVP, 100 mg of AA, and 9 mL of EG were mixed in a 50 mL three-neck flask and held at 110 °C in an oil bath under magnetic stirring for 1 h. The reaction temperature was then ramped to 200 °C in 30 min. The deposition of Pt atomic layers was initiated by injecting 13 mL of a Na$_2$PtCl$_6$ solution in EG (0.06 mg/mL) into the flask at a rate of 4.0 mL/h. For the concave decahedra with 47.5 wt % Pt, the Pt coating was formed by injecting 27 mL of the Na$_2$PtCl$_6$ solution in EG at a rate of 1.5 mL/h. After the Na$_2$PtCl$_6$ solution had been completely injected, the synthesis was continued at 200 °C for another 1 h. The solid product was collected by centrifugation, washed

once with acetone and five times with ethanol, and redispersed in 1 mL of DI water.

Etching of Pd from the Pd@Pt Concave Decahedra with 47.5 wt % Pt. In a typical procedure, 300 mg of KBr, 50 mg of PVP, 10 mg of FeCl$_3$, 0.06 mL of HCl, and 5.94 mL of DI water were mixed in a glass vial. The mixture was held at 90 °C in an oil bath under magnetic stirring, and then 0.1 mL of an aqueous suspension of the Pd@Pt concave decahedra was introduced. After etching for 2 or 3 h, the solid product was collected by centrifugation, followed by washing five times with ethanol and DI water.

Instrumentation. Transmission electron microscopy (TEM) images were taken using a Hitachi HT7700 microscope operated at 120 kV by drop casting the nanocrystal dispersions onto carbon-coated Cu grids and drying under ambient conditions. High-resolution high-angle annular dark-field scanning transmission electron microscopy (HAADF-STEM) and tomography images were carried out on a Cs-corrected FEI Titan 80/300 kV TEM/STEM microscope at ORNL. All STEM images were acquired using 300 kV and a beam size of ∼0.7 Å with a convergence angle of 30 mrad and collection angles of 65−220 mrad. The STEM tomography was conducted with an angular increment of 5° and a tilt range from 60° to −55°. Energy-dispersive X-ray (EDX) analyses were performed using a Hitachi HD-2700A Cs-corrected STEM/SEM microscope. The metal contents were measured using an inductively coupled plasma mass spectrometer (ICP-MS, NexION 300Q, PerkinElmer).

Preparation of the Working Electrodes. First, the Pd@Pt concave decahedra were loaded onto a carbon support (Ketjen Black EC-300J) with a metal loading content of 20% based on the total mass of Pd and Pt (determined by ICP-MS). Typically, 0.9 mg of the concave decahedra and 3.6 mg of Ketjen black were dispersed in 8 mL of ethanol under continuous ultrasonication for 3 h. The carbon-supported concave decahedra were then collected by centrifugation, redispersed in 10 mL of acetic acid, and heated at 60 °C for 12 h to clean the surface of the nanocrystals. The catalyst was recovered by centrifugation, followed by washing with ethanol twice. After being dried, 1.5 mg of the catalyst was redispersed in a mixture of 0.5 mL of DI water, 0.5 mL of isopropanol, and 20 μL of 5% Nafion under ultrasonication for 20 min. Twenty microliters of the suspension was then placed on a precleaned glassy carbon rotating disk electrode (RDE, Pine Research Instrumentation) with a geometric area of 0.196 cm^2 and dried at room temperature and under ambient conditions. The Tanaka Kinkinzoku Kogyo (TKK) Pt/C catalyst (46.1 wt % 2.8 nm Pt nanoparticles supported on Ketjen Black EC-300J) was used as a benchmark for comparison. Typically, 1.1 mg of the TKK catalyst was dispersed in a mixture of 0.5 mL of DI water, 0.5 mL of isopropanol, and 20 μL of 5% Nafion under ultrasonication for 20 min to produce an ink with a Pt concentration of 0.47 mg/mL (measured by ICP-MS). Ten microliters of the ink was then placed on a precleaned glassy carbon RDE and dried at room temperature and under ambient conditions.

Electrochemical Measurements. Electrochemical measurements were conducted using a glassy carbon RDE connected to a CHI 600E potentiostat (CH Instruments). Hydroflex hydrogen reference electrode (Gaskatel) and a Pt mesh were used as the reference electrode and counter electrode, respectively. All potentials were converted to values in reference to reversible hydrogen electrode (RHE). The electrolyte was 0.1 M HClO$_4$ prepared by diluting a 70% stock solution with DI water. The CV curve was recorded at room temperature in a N$_2$-saturated 0.1 M HClO$_4$ solution in the potential range of 0.08−1.1 V with a reference to the reversible hydrogen electrode (RHE), or V$_{RHE}$, at a scanning rate of 50 mV/s. We calculated the specific electrochemical active surface area (ECSA) of each catalyst on the basis of the charges associated with the desorption of hydrogen in the region of 0.08−0.45 V$_{RHE}$ after double-layer correction with a reference value of 210 μC/cm^2 for the desorption of a monolayer of hydrogen from Pt surfaces. We measured the ORR activities of catalysts at room temperature in the potential range of 0.08−1.1 V$_{RHE}$ in an O$_2$-saturated 0.1 M HClO$_4$ solution through the RDE method at a scanning rate of 10 mV/s (rotating rate of 1600 rpm). The background current was measured in the potential range of

0.08−1.1 V_{RHE} by running the ORR sweep profile in an N_2-saturated 0.1 M $HClO_4$ solution at a scanning rate of 10 mV/s (rotating rate of 1600 rpm). The ORR data were corrected by ohmic iR drop compensation and background currents. For the accelerated durability test, we performed CVs and ORR polarization curves after sweeping 5000 and 10 000 cycles in the range of 0.6 and 1.1 V_{RHE} at a rate of 0.1 V/s in an O_2-saturated 0.1 M $HClO_4$ solution at room temperature.

RESULTS AND DISCUSSION

Synthesis and Characterization of Pd@Pt Concave Decahedra. We first prepared Pd decahedral seeds with an average diameter of 19 nm (Figure S1a,b) by following a protocol recently developed in our group.[25] We then synthesized Pd@Pt concave decahedra using the polyol-based route developed for the fabrication of Pd@Pt$_{nL}$ (n = 1−6) core−shell, cubes, octahedra, and icosahedra.[18−20] Specifically, a solution of Na_2PtCl_6 (a precursor to Pt) in EG was slowly pumped into a suspension of the Pd decahedral seeds in EG held at 200 °C, in the presence of AA, PVP, and KBr. Different from the previous syntheses involving Pd cubic, octahedral, and icosahedral seeds, facets with a concave structure were formed on the surface of each decahedral seed (Figures S1c,d and S2) after the deposition of Pt atoms.

Figure 1a−c shows typical HAADF-STEM images of the Pd@Pt concave decahedra prepared by adding 13 mL of the
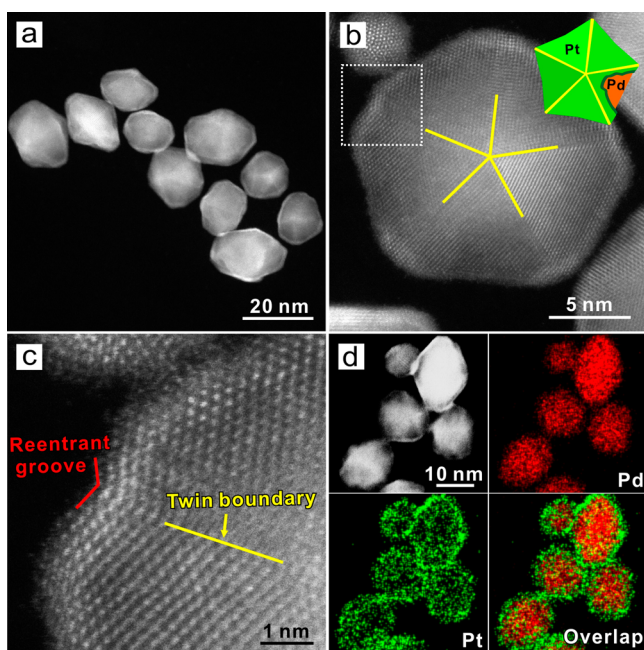

Figure 1. Structural and compositional analyses of the Pd@Pt core−shell concave decahedra with 29.6 wt % Pt. (a) HAADF-STEM image. (b) Atomic-resolution HAADF-STEM image and a model of the decahedron viewed along its 5-fold axis (inset). (c) Atomic-resolution HAADF-STEM image taken from the corner marked by a box in (b), showing the presence of re-entrant groove at a vertex and twin boundary along a ridge. (d) HAADF-STEM image of the concave decahedra and the corresponding EDX mapping of elemental Pd and Pt.

Na_2PtCl_6 solution. As indicated by the atomic-resolution image in Figure 1b, more Pt atoms were deposited on the vertices of each Pd decahedral seed than on the faces. On the basis of the data from ICP-MS (Table 1), the wt % of Pt in this sample was 29.6%, corresponding to an average shell thickness of about two

Table 1. Comparison of the Pt Deposition Efficiency (%) for the Pd@Pt Concave Decahedra

samples	wt % of Pt from ICP-MS	added Pt (mg)	deposited Pt (mg)	deposition efficiency (%)
Pd@Pt with 29.6 wt % Pt	29.6	0.361	0.302	83.7
Pd@Pt with 47.5 wt % Pt	47.5	0.562	0.489	87.0

atomic layers, if we assume a conformal and uniform Pt shell on the surface of each Pd decahedral seed. However, the atomic-resolution HAADF-STEM image shown in Figure 1c indicates that the thickness of the Pt shell at the vertex was about five atomic layers, whereas the thickness on the edge was noticeably thinner. Because the Pt shell adopted a concave structure on each face (Figure S3 and Table S1), the average shell thickness should be thinner than two atomic layers on top of the {111} facets. The twin planes could still be easily resolved in the core−shell decahedron, as marked by the yellow lines in Figure 1b and c, implying that the twin defects on the original Pd decahedral seed were well preserved during Pt deposition. Additionally, we observed re-entrant grooves present at some vertices of the core−shell nanocrystals (Figure 1c), which might have been formed to effectively relax the internal strain of the pentagonal crystal.[26] We also used EDX mapping to confirm the formation of a core−shell structure for the nanocrystals. As shown in Figure 1d, Pd and Pt were only detected from the cores and shells, respectively, of the concave decahedra.

By reducing the injection rate to 1.5 mL/h and increasing the volume of Na_2PtCl_6 solution to 27 mL, we obtained Pd@Pt concave decahedra with 47.5 wt % Pt, as indicated by ICP-MS analysis. As illustrated by the HAADF-STEM images in Figure 2a and b, the nanocrystals also clearly showed a concave structure on the surface, with more Pt being deposited at the vertices of each decahedral seed relative to the faces. The atomic-resolution HAADF-STEM image indicates that the Pt shell at the vertex was increased to about seven atomic layers in thickness, while the Pt shell deposited on the edges along the ⟨100⟩ direction was about five atomic layers (Figure 2c). From the ICP-MS data, we calculated an average thickness of approximately four atomic layers by assuming a conformal, uniform Pt shell. Given the concave structure, the average thickness of the Pt skins on the {111} facets should therefore be less than four atomic layers. The concave structure could be better resolved using HAADF-STEM tomography. As shown by the image in Figure 2c and the images in Figure S4 (captured at different tilting angles), the Pd@Pt decahedra clearly exhibited a concave structure on each facet (see Movie S1 for a video of the images recorded at different tilting angles). Furthermore, EDX mapping of the Pd and Pt elements (Figure 2d) confirmed the formation of a Pd@Pt core−shell configuration for the nanocrystals.

Mechanistic Investigation of the Formation of Pd@Pt Concave Decahedra. Figure 3 shows a plausible mechanism responsible for the formation of the concave decahedra. For clarity, we refer to the 10 edges along twin boundaries as "ridges" and the five edges covered by {100} facets as "edges" (Figure 3a). There are also two different types of vertices on a decahedron. Five of the vertices are oriented along the ⟨211⟩ direction, and each one of them is intersected by two twin boundaries. These are defined as "type-A" vertices. The remaining two vertices are oriented along the ⟨110⟩ direction,
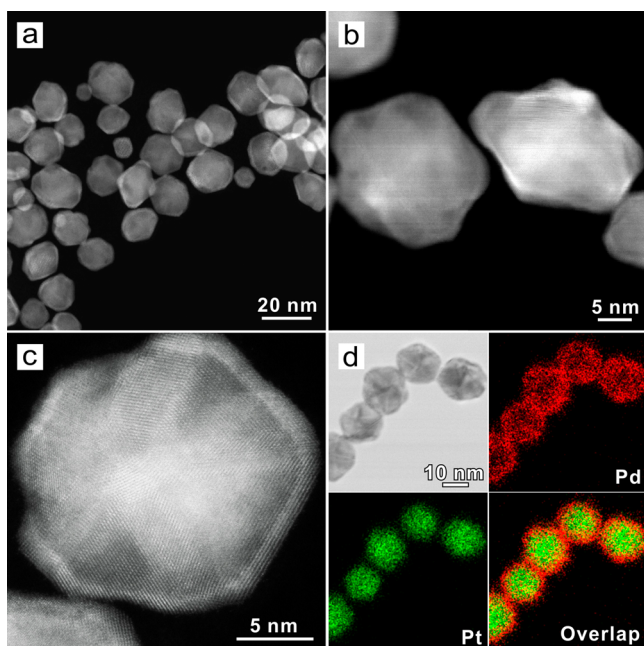
Figure 2. Structural and compositional analyses of the Pd@Pt core–shell concave decahedra with 47.5 wt % Pt. (a) Low- and (b) high-magnification HAADF-STEM images of the decahedra, showing that more Pt was deposited on the vertices and edges of a Pd decahedral seed than the faces. (c) Atomic-resolution HAADF-STEM image of an individual decahedron. (d) HAADF-STEM image of the concave decahedra and the corresponding EDX mapping of elemental Pd and Pt.
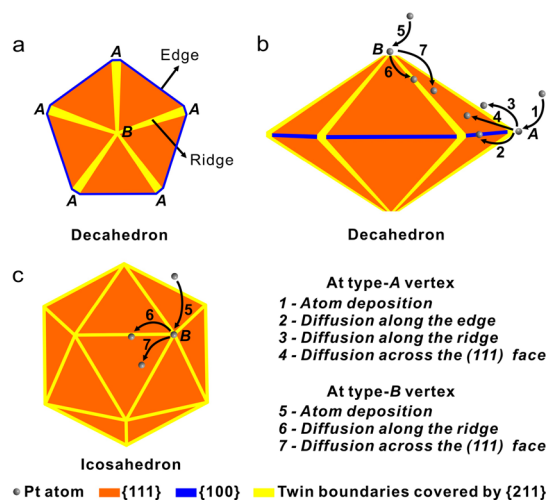

Figure 3. (a) Schematic of a decahedron viewed along its 5-fold axis, showing the type-*A* and type-*B* vertices, as well as the ridges and edges. (b,c) Schematic illustrations showing how the Pt atoms are deposited onto Pd decahedral and icosahedral seeds, respectively, and the possible routes for the initially deposited Pt atoms to diffuse across the surface.

and each of them is intersected by five twin boundaries. We refer to these as "type-*B*" vertices in our discussion. As demonstrated in our previous work,[27] the growth pattern and thus the final shape or morphology of a nanocrystal are determined by the relative rates for the deposition of atoms and the diffusion of adatoms. Because of the involvement of a strong reducing agent based on AA and an elevated temperature, the Pt(IV) precursor should be reduced to

Pt(0) atoms immediately upon its introduction into the reaction solution. Therefore, the primary factor that controls the rate of atom deposition in this system should be the same as the injection rate used for the Pt precursor solution.

Although decahedra and icosahedra possess similar twin defects on their surfaces, the Pt atoms showed completely different behaviors when they were deposited onto Pd decahedral and icosahedral seeds under identical experimental conditions. Whereas the Pt atoms formed a conformal, uniform shell over an icosahedral seed,[20] they instead developed into a concave structure on a decahedral seed even at the same reaction temperature of 200 °C. When comparing the structures of icosahedra and decahedra, it is worth noting that an icosahedron only contains type-*B* vertices and ridges while a decahedron contains both types of vertices as well as ridges and edges (Figure 3b and c). When Pt atoms are deposited onto the type-*B* vertices of a Pd icosahedron (Figure 3b), they can readily diffuse along the ridges and across {111} facets at a relatively high temperature of 200 °C, resulting in the formation of a conformal, uniform Pt shell.[20] In the case of a decahedron, however, while the Pt atoms deposited on the type-*B* vertices can adopt the same diffusion mode as for an icosahedron, those deposited on the type-*A* vertices tend to take a different route.

There are three different diffusion pathways for the Pt atoms deposited on the type-*A* vertex of a Pd decahedral seed: (i) along the edges, (ii) along the ridges, and (iii) across the {111} faces. Because of the relatively high energies associated with the ridges (due to twin defects) and edges (due to the square packing for the {100} facets), the Pt atoms deposited at the type-*A* vertex tend to diffuse to edges and ridges and then stay at these sites. As a result, when 13 mL of the Pt precursor solution was injected at a rate of 4 mL/h, even at a temperature as high as 200 °C, the Pt atoms still were unable to spread over the entire surface of a decahedral seed to generate a uniform shell. When increasing the volume of Pt precursor solution to 27 mL at the same injection rate of 4 mL/h, we obtained both concave decahedra and multipods with a decahedral shape (Figure S5a). The multipods were formed because of inadequate diffusion of Pt adatoms from the vertices to edges relative to the rate of deposition, further implying that the Pt atoms were initially deposited on the vertices of a Pd decahedral seed, and subsequently allowed to diffuse to ridges, edges, and faces. By lowering the injection rate to 1.5 mL/h, and thereby decreasing the Pt deposition rate, we obtained concave decahedra with 47.5 wt % Pt (Figures 2 and S5b).

We also studied the effect of reaction temperature on the morphology of the particles. When the reaction temperature was reduced to 140 °C, the product still adopted a concave structure similar to that obtained at 200 °C (Figure S5c). However, the weight percentage of Pt in the product dropped to 20.4% (according to ICP-MS analysis) due to the decreased reducing power of AA at a lower temperature. When the reaction temperature was further reduced to 110 °C, we found that the edges of most particles in the product became more rounded (Figure S5d). The facets corresponding to the twin boundaries (i.e., ridges) on a decahedron can be indexed as {211} facets, while the facets corresponding to the edges can be indexed as {100} facets.[28] Calculations have shown that the surface energy of Pd(100) (1661 ergs/cm^2) is slightly higher than that of Pd(211) (1617 ergs/cm^2), whereas the Pd(111) (1382 ergs/cm^2) is much lower than both Pd(100) and Pd(211) in terms of surface energy.[29] In addition, the rate of

diffusion of an adatom across a surface is determined by the diffusion coefficient (D), which can be expressed as $D = D_0 \exp(-E_{diff}/RT)$. In this equation, D_0 is the pre-exponential factor, E_{diff} is the energy barrier to diffusion, R is the ideal gas constant, and T is the absolute temperature.[27] Therefore, at a low temperature of 110 °C, Pt atoms deposited at type-*B* vertices tend to diffuse along the edges, remaining at these sites and forming more rounded edges to minimize both the internal strain and the total surface free energy.[30] When conducted at 200 °C, the temperature is sufficiently high for Pt atoms deposited at type-*B* vertices to overcome the diffusion energy barriers and access both ridges and edges.

To further confirm the core–shell structure, we tried to etch away the Pd cores from the Pd@Pt concave decahedra with 47.5 wt % Pt. The etching protocol was similar to what was used in the synthesis of Pt cubic and octahedral nanocages.[12] After etching at 90 °C for 2 h, we were able to selectively remove the Pd cores to obtain Pt-based decahedral nanocages with a Pt content of 85 wt % as shown by ICP-MS analysis (Figure 4a), confirming that the original Pd@Pt concave
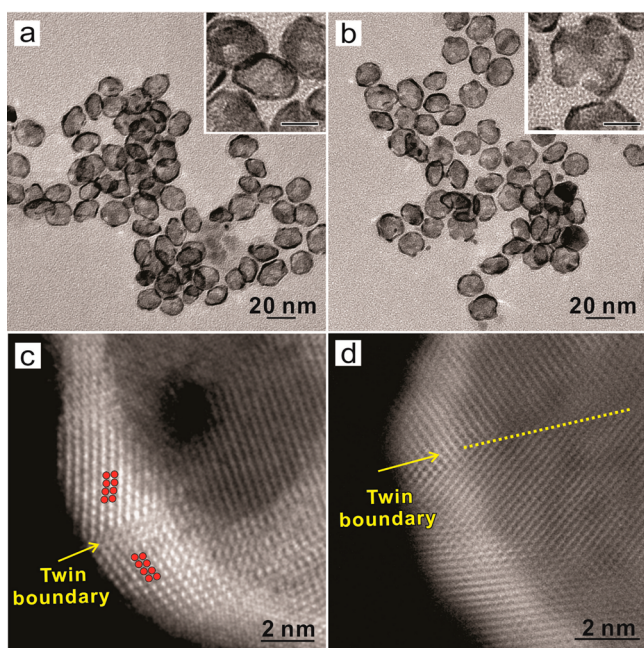

Figure 4. (a,b) TEM image of Pt nanocages obtained by selectively etching away Pd cores from the Pd@Pt concave decahedra with 47.5 wt % Pt for (a) 2 h and (b) 3 h, respectively. The scale bars in the insets are 10 nm. (c,d) Atomic resolution HAADF-STEM images taken from two different particles in sample (a), showing the preservation of the twin defect at a type-*A* vertex and along a ridge of the decahedral nanocage.

decahedra indeed had a core–shell structure. When the etching time was extended to 3 h (Figure 4b), the content of Pt in the product maintained a similar value of 84.6 wt % according to ICP-MS analysis. However, some of the {111} facets were also etched away, whereas the majority of Pt atoms on the edges/ridges and vertices of the decahedra were retained. This result also demonstrates that more Pt atoms were deposited on the vertices and edges/ridges of the Pd decahedral seeds than on the faces to generate a concave structure. Interestingly, atomic-resolution HAADF-STEM images (Figure 4c and d) confirmed that the twin defects were preserved after the Pd cores had been etched away.

Electrochemical Measurements. We evaluated the catalytic activities of both of the Pd@Pt concave decahedra with 29.6 and 47.5 wt % Pt toward ORR by benchmarking against a commercial Pt/C catalyst from TKK. Figure 5a shows cyclic voltammograms (CVs) of the three different types of catalysts. The ECSAs of the catalysts were calculated from the charges associated with the desorption of hydrogen between 0.08 and 0.45 V_{RHE}. The specific ECSA of a catalyst was obtained by normalizing against the Pt mass (Table S2). The specific ECSAs of both catalysts based on concave decahedra were found to be comparable to that of the Pt/C (88.9 m^2/g), although the concave decahedra were more than 7 times larger than the Pt nanoparticles in the commercial Pt/C. In particular, due to a higher dispersion of Pt atoms on the surfaces of concave decahedra with 29.6 wt % Pt, the specific ECSA (95.9 m^2/g) of this catalyst was even slightly higher than that of the Pt/C. These results suggest that the dispersion of Pt atoms could be retained when deposited on Pd decahedra as ultrathin shells.

Figure 5b shows the positive-going ORR polarization curves of the catalysts. The mass and specific activities ($j_{k,mass}$ and $j_{k,specific}$) were calculated using the Koutecky–Levich equation and then normalized against the ECSA and Pt mass of the catalyst. Both the specific and the mass activities of the concave decahedra were greatly enhanced in the potential region of 0.86–0.94 V_{RHE}; the concave decahedra with 29.6 wt % Pt exhibited the highest activities (Figure S6). At 0.9 V_{RHE}, the $j_{k,specific}$ and $j_{k,mass}$ of the concave decahedra with 29.6 wt % Pt were 1.66 mA/cm$^2_{Pt}$ and 1.60 A/mg$_{Pt}$, respectively (Figure 5c and d). In terms of specific activity, the concave decahedra with 29.6 wt % Pt showed an enhancement factor of 4.6 relative to that of the commercial Pt/C (0.36 mA/cm$^2_{Pt}$). The enhancement in specific activity can be partially attributed to the ligand effect and the strain arising from the lattice mismatch between Pd and Pt.[18−20,31−34] In addition, nanocrystals with a concave structure and thus high-index facets should contain more unsaturated steps, edges, kinks, and low-coordination atoms on the surface, which are more favorable for the adsorption of O$_2$ molecule.[5] All of these factors may contribute to the markedly enhanced specific activity observed for the Pd@Pt concave decahedra. As a critical indicator for the commercialization viability of a Pt-based catalyst, the $j_{k,mass}$ of the concave decahedra with 29.6 wt % Pt at 0.9 V_{RHE} was 5 times that of the Pt/C (0.32 A/mg$_{Pt}$). In terms of precious metals (both Pd and Pt), the mass activity of the concave decahedra with 29.6 wt % Pt still showed 1.5-fold enhancement as compared to that of the commercial Pt/C. Clearly, it is the improvements in both specific ECSA and specific activity that contributed to the drastically enhanced mass activity measured for the concave decahedra with 29.6 wt % Pt.

We also evaluated the long-term catalytic stability of the concave decahedra with 29.6 wt % Pt through an accelerated durability test at room temperature (Figure 6). The concave decahedra showed substantial improvement in durability as compared to the TKK Pt/C. After 5000 cycles, the specific ECSA of the concave decahedra dropped less than 1%, while the specific ECSA of the Pt/C decreased by 31% (Figure 6a). Even after 10 000 cycles, the specific ECSA of the concave decahedra only dropped by 21%, while the specific ECSA of the Pt/C decreased by 40%. The slower deterioration in specific surface area can be attributed to a much larger size for the concave decahedra relative to the Pt nanoparticles in the Pt/C catalyst (19.4 nm vs 2.8 nm). After 10 000 cycles, the mass
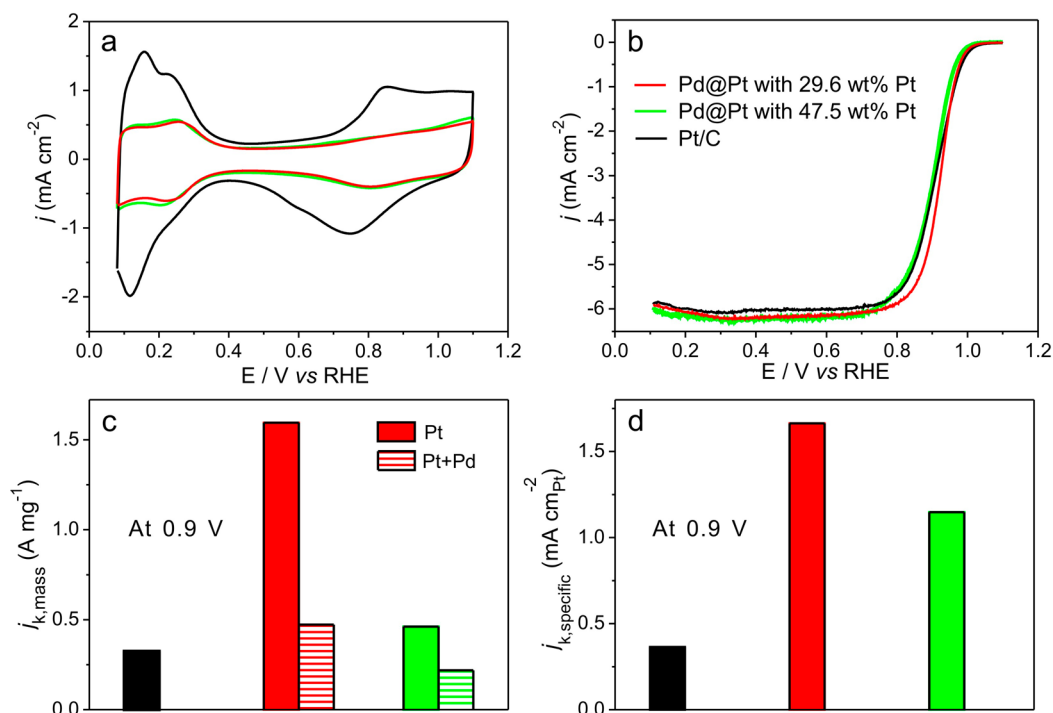
Figure 5. Electrochemical properties of the carbon-supported Pd@Pt concave decahedra with 29.6 and 47.5 wt % Pt, respectively, benchmarked against the TKK Pt/C catalyst. (a) CVs of the catalysts in a N_2-saturated $HClO_4$ solution at room temperature. (b) Positive-going ORR polarization curves of the catalysts in an O_2-saturated $HClO_4$ solution. (c) Mass and (d) specific ORR activities at 0.9 V_{RHE}, which are presented as kinetic current density (j_k) normalized to the mass of Pt (or Pd+Pt) and ECSA, respectively, of the catalyst. The color scheme in (b) applies to all other panels.
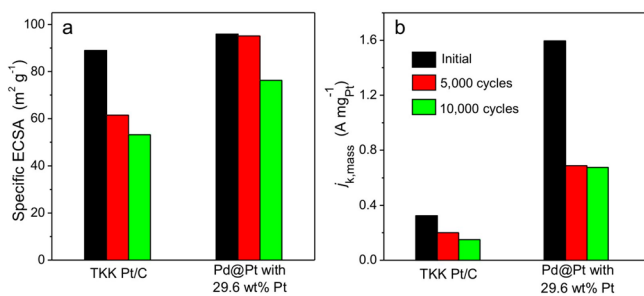
Figure 6. Durability tests for the carbon-supported Pd@Pt concave decahedra with 29.6 wt % Pt and the TKK Pt/C catalyst. The comparison is based on (a) the specific ECSA and (b) the mass ORR activity at 0.9 V_{RHE} for the catalysts before and after the accelerated durability test. The color scheme specified in (b) applies to both panels.

activity of the concave decahedra at 0.9 V_{RHE} decreased to 0.69 A/mg$_{Pt}$, still providing 2.2-fold enhancement when compared to the pristine TKK Pt/C. In contrast, the mass activity of the Pt/C had dropped to 0.15 A/mg$_{Pt}$ (Figure 6b). The Pd@Pt concave decahedra were transformed into cage-like structures made of Pt during the accelerated durability via the selective removal of Pd cores (Figure S7). The dissolution of Pt was largely prevented due to its higher chemical stability relative to Pd. The loss of Pd diminished the ligand and strain effects, causing the specific activity to decrease. These results demonstrate that both the activity and the durability of a Pt-based ORR catalyst can be improved by forming a core–shell structure with an ultrathin shell and a concave surface.

CONCLUSIONS

In summary, we have fabricated multiply twinned Pd@Pt concave decahedra by coating the surfaces of presynthesized Pd decahedral seeds with Pt atoms. As opposed to the uniform deposition of Pt on Pd icosahedral seeds, the Pt atoms were deposited on Pd decahedra as ultrathin shells with a concave surface even when the reaction was conducted at a temperature as high as 200 °C. Because of the presence of twin boundaries, the Pt atoms were preferentially deposited onto the vertices of a Pd decahedral seed, followed by surface diffusion along the edges/ridges and then across to the faces. The {100} and {211} facets on the edges/ridges of a decahedron tend to trap the Pt adatoms at these high-energy sites, resulting in the formation of a Pt shell containing multiple concave facets. The concave decahedra with 29.6 wt % Pt showed greatly enhanced activity and durability toward ORR when compared to a commercial Pt/C catalyst. Specifically, the enhancement in specific activity can be attributed to a combination of ligand effect, strain effect arising from the lattice mismatch between Pd and Pt, and the high-index facets associated with a concave surface. Together with the large specific ECSA arising from an ultrathin Pt shell, the enhancement in specific activity led to a markedly increased mass activity. After 10 000 cycles of accelerated durability test, the Pd@Pt concave decahedra still showed a mass activity twice that of the pristine Pt/C, although they were transformed into Pt-based nanocages due to the selective removal of the Pd cores via electrochemical etching. The multiply twinned concave decahedra represent a new class of attractive structures for the development of cost-effective and high-performance catalysts toward ORR and other types of reactions.

■ ASSOCIATED CONTENT

ⓈSupporting Information

The Supporting Information is available free of charge on the ACS Publications website at DOI: 10.1021/jacs.5b10059.

TEM image and size distribution plot of the Pd decahedral seeds; TEM and SEM images of the Pd@Pt concave decahedra with 29.6 and 47.5 wt % Pt; atomic resolution HAADF-STEM image of a Pd@Pt core−shell concave decahedron with 29.6 wt % Pt viewed along its 5-fold axis; HAADF-STEM tomography tilt series of the concave decahedra with 47.5 wt % Pt; TEM images of the products obtained at a faster injection rate of 4 mL/h for the precursor or at lower reaction temperatures of 110 and 140 °C than the standard protocol for the synthesis of concave decahedra with 47.5 wt % Pt; mass and specific activities given as kinetic current densities; TEM images of the concave decahedra with 29.6 wt % Pt supported on carbon before and after the accelerated durability test; a table of calculated angles between high-index {hkk} facets and the {100} edge facets; and a table of specific ECSAs for the catalysts based on the concave decahedra and Pt/C (PDF)

Tomographic video of HAADF-STEM images of the concave decahedra with 47.5 wt % Pt taken at different tilt angles (AVI)

■ AUTHOR INFORMATION

Corresponding Author

*younan.xia@bme.gatech.edu

Notes

The authors declare no competing financial interest.

■ ACKNOWLEDGMENTS

■ REFERENCES

(1) Debe, M. K. Nature 2012, 486, 43−51.
(2) Gasteiger, H. A.; Kocha, S. S.; Sompalli, B.; Wagner, F. T. Appl. Catal., B 2005, 56, 9−35.
(3) Chen, J.; Lim, B.; Lee, E. P.; Xia, Y. Nano Today 2009, 4, 81−95.
(4) Department of Energy. Multi-Year Research, Development and Demonstration Plan; http://www.eere.energy.gov, 2014.
(5) Yu, T.; Kim, D. Y.; Zhang, H.; Xia, Y. Angew. Chem., Int. Ed. 2011, 50, 2773−2777.
(6) Zhou, W.; Wu, J.; Yang, H. Nano Lett. 2013, 13, 2870−2874.
(7) Zhang, J.; Gan, L.; Fang, J.; Zou, S. Nano Lett. 2010, 10, 638−644.
(8) Choi, S.-I.; Xie, S.; Shao, M.; Odell, J. H.; Lu, N.; Peng, H.; Protsailo, L.; Guerrero, S.; Park, J.; Xia, X.; Wang, J.; Kim, M. J.; Xia, Y. Nano Lett. 2013, 13, 3420−3425.
(9) Wu, J.; Qi, L.; You, H.; Gross, A.; Li, J.; Yang, H. J. Am. Chem. Soc. 2012, 134, 11880−11883.
(10) Cui, C.; Lin, G.; Heggen, M.; Rudi, S.; Strasser, P. Nat. Mater. 2013, 12, 765−771.
(11) Chen, C.; Kang, Y.; Huo, Z.; Zhu, Z.; Huang, W.; Xin, H. L.; Snyder, J. D.; Li, D.; Herron, J. A.; Mavrikakis, M.; Chi, M.; More, K. L.; Li, Y.; Markovic, N. M.; Somorjai, G. A.; Yang, P.; Stamenkovic, V. R. Science 2014, 343, 1339−1343.
(12) Zhang, L.; Roling, L. T.; Wang, X.; Vara, M.; Chi, M.; Liu, J.; Choi, S.-I.; Park, J.; Herron, J. A.; Xie, Z.; Mavrikakis, M.; Xia, Y. Science 2015, 349, 412−416.
(13) Zhang, J.; Vukmirovic, M. B.; Xu, Y.; Mavrikakis, M.; Adzic, R. R. Angew. Chem., Int. Ed. 2005, 44, 2132−2135.
(14) Adzic, R. R.; Zhang, J.; Sasaki, K.; Vukmirovic, M. B.; Shao, M.; Wang, J. X.; Nilekar, A. U.; Mavrikakis, M.; Valerio, J. A.; Uribe, F. Top. Catal. 2007, 46, 249−262.
(15) Sasaki, K.; Naohara, H.; Choi, Y.; Cai, Y.; Chen, W.-F.; Liu, P.; Adzic, R. R. Nat. Commun. 2012, 3, 1115.
(16) Zhang, J.; Mo, Y.; Vukmirovic, M. B.; Klie, R.; Sasaki, K.; Adzic, R. R. J. Phys. Chem. B 2004, 108, 10955−10964.
(17) Koenigsmann, C.; Santulli, A. C.; Gong, K.; Vukmirovic, M. B.; Zhou, W.-P.; Sutter, E.; Wong, S. S.; Adzic, R. R. J. Am. Chem. Soc. 2011, 133, 9783−9795.
(18) Xie, S.; Choi, S.-I.; Lu, N.; Roling, L. T.; Herron, J. A.; Zhang, L.; Park, J.; Wang, J.; Kim, M. J.; Xie, Z.; Mavrikakis, M.; Xia, Y. Nano Lett. 2014, 14, 3570−3576.
(19) Park, J.; Zhang, L.; Choi, S.-I.; Roling, L. T.; Lu, N.; Herron, J. A.; Xie, S.; Wang, J.; Kim, M. J.; Mavrikakis, M.; Xia, Y. ACS Nano 2015, 9, 2635−2647.
(20) Wang, X.; Choi, S.-I.; Roling, L. T.; Luo, M.; Ma, C.; Zhang, L.; Chi, M.; Liu, J.; Xie, Z.; Herron, J. A.; Mavrikakis, M.; Xia, Y. Nat. Commun. 2015, 6, 7594.
(21) Xia, Y.; Xiong, Y.; Lim, B.; Skrabalak, S. E. Angew. Chem., Int. Ed. 2009, 48, 60−103.
(22) Quan, Z.; Wang, Y.; Fang, J. Acc. Chem. Res. 2013, 46, 191−202.
(23) Tian, N.; Zhou, Z.-Y.; Sun, S.-G.; Ding, Y.; Wang, Z. L. Science 2007, 316, 732−735.
(24) Jin, M.; Zhang, H.; Xie, Z.; Xia, Y. Angew. Chem., Int. Ed. 2011, 50, 7850−7854.
(25) Huang, H.; Wang, Y.; Ruditskiy, A.; Peng, H.-C.; Zhao, X.; Zhang, L.; Liu, J.; Ye, Z.; Xia, Y. ACS Nano 2014, 8, 7041−7050.
(26) Zhang, W.; Liu, Y.; Cao, R.; Li, Z.; Zhang, Y.; Tang, Y.; Fan, K. J. Am. Chem. Soc. 2008, 130, 15581−15588.
(27) Xia, X.; Xie, S.; Liu, M.; Peng, H.-C.; Lu, N.; Wang, J.; Kim, M. J.; Xia, Y. Proc. Natl. Acad. Sci. U. S. A. 2013, 110, 6669−6673.
(28) Choi, S.-I.; Herron, J. A.; Scaranto, J.; Huang, H.; Wang, Y.; Xia, X.; Lv, T.; Park, J.; Peng, H.-C.; Mavrikakis, M.; Xia, Y. ChemCatChem 2015, 7, 2077−2084.
(29) Zhang, J.-M.; Ma, F.; Xu, K.-W. Appl. Surf. Sci. 2004, 229, 34−42.
(30) Yacaman, M. J.; Ascencio, J. A.; Liu, H. B.; Gardea-Torresdey, J. J. Vac. Sci. Technol., B: Microelectron. Process. Phenom. 2001, 19, 1091−1103.
(31) Kitchin, J. R.; Nørskov, J. K.; Barteau, M. A.; Chen, J. G. Phys. Rev. Lett. 2004, 93, 156801−156804.
(32) Wang, J. X.; Inada, H.; Wu, L.; Zhu, Y.; Choi, Y.; Liu, P.; Zhou, W.-P.; Adzic, R. R. J. Am. Chem. Soc. 2009, 131, 17298−17302.
(33) Wang, X.; Orikasa, Y.; Takesue, Y.; Inoue, H.; Nakamura, M.; Minato, T.; Hoshi, N.; Uchimoto, Y. J. Am. Chem. Soc. 2013, 135, 5938−5941.
(34) Mavrikakis, M.; Hammer, B.; Nørskov, J. K. Phys. Rev. Lett. 1998, 81, 2819−2822.